GSA Data Repository 2018001

Pulsed magmatic fluid release for the formation of porphyry deposits: tracing fluid evolution in absolute-time from the Tibetan Qulong Cu-Mo deposit

Yang Li [1,2*], **Xian-Hua Li** [2], **David Selby** [1] and **Jian-Wei Li** [3]

[1] Department of Earth Sciences, Durham University, DH1 3LE, Durham, UK

[2] State Key Laboratory of Lithospheric Evolution, Institute of Geology and Geophysics, Chinese Academy of Sciences, 10029, Beijing, China

[3] State Key Laboratory of Geological Processes and Mineral Resources, China University of Geosciences, 430074, Wuhan, China

Corresponding author now at Department of Geology and Geophysics, Yale University, New Haven, 06511, USA. Email Address: yang.li@yale.edu; cugliyang@126.com.

Table of Contents

A1. List of supplementary tables and figures

Table DR1. Oxygen isotopic composition of quartz grains co-precipitated with molybdenite, with calculated estimates of the $\delta^{18}O_{fluid}$ and magmatic water percentage contribution at vein formation temperatures of 420 ^{o}C, 350 ^{o}C and 300 ^{o}C, respectively.

Table DR2. SIMS $\delta^{18}O$ values of magmatic zircon and quartz grains of the Rongmucuola pluton.

Table DR3. SIMS $\delta^{18}O$ values of hydrothermal quartz from Qulong.

Figure DR1. Geological setting of the Lhasa terrane and deposit geology map of the Qulong porphyry Cu-Mo deposit. A) Simplified geological setting of the Lhasa terrane, Gangdese Magmatic Belt and Gangdese Porphyry Copper Deposits Belt. B) Geological map of the Qulong porphyry Cu-Mo deposit. C) Cross section showing the crosscutting relationship of the Miocene units of the Qulong porphyry Cu-Mo deposit. Simplified and revised from Zhao et al. (2016) and Li et al. (2017b).

Figure DR2. Plot of $\delta^{18}O_{(quartz)}$ vs. $\delta^{18}O_{(zircon)}$ of the Rongmucuola pluton at Qulong. The zircon and quartz grains are in equilibrium at ~674 ± 151 ^{o}C, which closely represent magmatic values. The equilibrium equation is from Trail et al. (2009). See text for details.

Figure DR3. Representative quartz veins, CL images of quartz grains and SIMS oxygen isotope data of the studied samples. A) Sinusoidal quartz vein represents the formation during the semi-solid crystalline state of the aplite intrusion before the main stage mineralization. B) CL images of quartz grains from A with positions of SIMS analysis; the green box highlights the resorption and dissolution of the CL-dark core, which is overprinted by CL-bright overgrowth rim. C) SIMS $\delta^{18}O$ plot of the three transects in B. D) Main mineralization stage representative molybdenite bearing quartz vein. E) CL image of quartz grains selected from

D with positions of SIMS analysis. Insert shows quartz grains enclosing molybdenite grains used for CL imaging and SIMS analysis. F) $\delta^{18}O$ plot of quartz grains from E showing homogeneous oxygen isotopic composition, with the $\delta^{18}O$ values being independent of the presence/absence of micro-fractures. G) Sketch shows the sampling strategy to obtain fluid inclusion, Re-Os, and SIMS quartz oxygen isotopic data from the same vein. This figure is an expanded version of Figure 2 in the main text.

Figure DR4. Oxygen diffusion time and equilibrium time between quartz and water. A) Time for a 400 μm quartz grain (diffusion distance is 200 μm) to reach complete oxygen diffusion exchange at different temperatures under hydrous conditions. The diffusion coefficient at 500 and 400 ^{o}C are from Valley and Graham (1996) with the rest presented as interpolations. B) Growth time for a 400 μm quartz grain at variable temperatures, and time needed for the grain to reach oxygen equilibrium with fluid at 300 ^{o}C with a salinity of 5.8 NaCl equiv. %, and mineral/water ratio of 5. Growth speed and the equilibrium time are from Pollington et al. (2016) and Cole et al. (1992), respectively.

Figure DR5. SIMS $\delta^{18}O$ values of hydrothermal quartz (co-genetic with molybdenite) analyzed at Qulong, with an absolute timeframe determined by molybdenite Re-Os dating (Li et al., 2017a). Fluid $\delta^{18}O$ values are calculated using formation temperatures determined from a fluid inclusion study (Li et al., 2017b). Fluid $\delta^{18}O$ values are also calculated at hypothesized temperatures of at 420, 350 and 300 ^{o}C, which are the upper, average and lower limits of mineralization temperature at Qulong and PCD in general (Richards, 2011; Kouzmanov and Pokrovski, 2012). Also presented is the magmatic water percentage contribution at these variable temperatures. The $\delta^{18}O_{fluid}$ and magmatic water contribution trends demonstrate the presence of three intermittent pulses, and show a continuous drop in the flux of magmatic

derived fluid during ore formation. This figure is an expanded version of Figure 3 in the main text.

A2. Geological framework of Qulong

Qulong is China's largest porphyry Cu-Mo deposit, containing 11 Mt of Cu and 0.6 Mt of Mo (Li et al., 2017b). The deposit geology has been extensively studied and is summarized here. The Qulong deposit occurs in the eastern Gangdese porphyry copper belt that hosts tens of porphyry copper systems (Fig. DR1A). The deposit geology is dominated by Jurassic volcanic/intrusive rocks and Miocene porphyries (Yang et al., 2009; Xiao et al., 2012; Hu et al., 2015; Zhao et al., 2016; Li et al., 2017a; Li et al., 2017b). The order of emplacement of the Mid-Miocene ore related intrusions is observed to be the pre-ore Rongmucuola monzogranite pluton, syn-ore aplite and monzogranite P porphyry, monzogranite X porphyry, and finally the post-ore quartz diorite (Fig. DR1B-C). In addition, a syn-ore hydrothermal breccia pipe, comprising two stages of breccia, developed following the emplacement of the X porphyry. High precision zircon U-Pb dating suggests that the Rongmucuola pluton, P porphyry and quartz-diorite were emplaced at 17.142 ± 0.023 Ma (including ^{238}U decay constant uncertainty), 16.009 ± 0.024 Ma and 15.166 ± 0.020 Ma, respectively (Li et al., 2017a).

The Cu-Mo mineralization at Qulong is predominately hosted by the western Rongmucuola pluton with a small portion of ore occurring in the Jurassic volcanic rocks (Fig. DR1B). Mineralization is spatially associated with potassic and, to a lesser extent, with propylitic and phyllic alteration assemblages (Yang et al., 2009; Li et al., 2017a; Li et al., 2017b). The potassic alteration assemblages are characterized by K-feldspar and biotite in the center of the deposit with the most intensive alteration spatially associated with the P porphyry and the north-south fault. Propylitic alteration assemblages are widely distributed in

89 the western Rongmucuola pluton and overprint the potassic alteration assemblages, which are
90 best illustrated by the selective replacement of biotite and plagioclase by chlorite bearing
91 selvages. Phyllic alteration assemblages are represented by the pervasive replacement of
92 feldspar by fine-grained sericite and ultra-fine granular quartz, and occur ubiquitous in the
93 western Rongmucuola pluton and overprint most of the potassic and propylitic alteration
94 assemblages.

95 The main ore minerals are chalcopyrite and molybdenite which occur predominately in
96 veinlets, which are classified as A-type, B-type and D-type veins, with B-type veins being the
97 most abundant and hosting the majority of the Cu-Mo mineralization (Yang et al., 2009; Li et
98 al., 2017a). Previous high precision Re-Os geochronology (Li et al., 2017a) demonstrates that
99 the majority of metals at Qulong were precipitated within 266 ± 13 kyrs between 16.126 ±
100 0.077 and 15.860 ± 0.075 Ma (including ^{187}Re decay constant uncertainty). Coupling the high
101 precision dating, vein types and cooling history indicates that the mineralization process
102 comprise three short-lived (38 - 59 kyrs) pulses between 16.126 ± 0.008 and 16.050 ± 0.005
103 Ma, 16.040 ± 0.007 and 15.981 ± 0.007 Ma, and ~15.981 ± 0.007 and 15.860 ± 0.010 Ma.
104 With vein formation ages and temperatures constrained by molybdenite Re-Os dating and
105 fluid inclusion analysis (Li et al., 2017a; Li et al., 2017b), respectively, the cooling rate of the
106 Qulong hydrothermal system has been constrained to be 0.55 ± 0.11 ^{o}C/kyr, with much faster
107 cooling rates (~1.2 ^{o}C/kyr) for the individual mineralization pulses.

108 **A3. Samples and analytical methods**

109 **A3.1 Samples**

110 The selected sample-set were quartz-molybdenite veinlets which have been previously
111 studied in detail; with formation ages and temperatures (Table DR1) constrained by high

112 precision molybdenite Re-Os dating and fluid inclusion studies (Li et al., 2017a; Li et al.,
113 2017b). The formation ages of these veins (n = 12) were 16.126 ± 0.008 Ma, (2σ, analytical
114 uncertainty), 16.107 ± 0.015 Ma, 16.098 ± 0.013 Ma, 16.088 ± 0.007 Ma, 16.050 ± 0.005
115 Ma, 16.040 ± 0.007 Ma, 16.036 ± 0.012 Ma, 16.011 ± 0.015 Ma, 15.981 ± 0.007 Ma, 15.943
116 ± 0.007 Ma, 15.939 ± 0.006 Ma, and 15.860 ± 0.010 Ma, with vein formation temperatures
117 (trapping temperatures of fluid inclusion groups) of 425 ± 20 ^{o}C, 398 ± 20 ^{o}C, 390 ± 20 ^{o}C,
118 380 ± 20 ^{o}C, 360 ± 20 ^{o}C, 365 ± 20 ^{o}C, 365 ± 20 ^{o}C, 340 ± 20 ^{o}C, 290 ± 20 ^{o}C, 345 ± 20 ^{o}C,
119 310 ± 20 ^{o}C, 280 ± 20 ^{o}C, respectively.

120 Quartz grains closely associated with molybdenite grains from the parallel chips (Fig.
121 DR3G) of the veinlets (Fig. 2B, Fig. DR3D) were recovered during the molybdenite
122 separation process (Li et al., 2017a) for SIMS oxygen isotope analysis (Fig. DR3G). The
123 textural association between the quartz and molybdenite (Fig. DR3D-E) and previous fluid
124 inclusion study (Li et al., 2017b) suggested that these minerals were co-precipitated, which
125 permit the linkage of the nature of the fluid recorded in the quartz to the timing of the ore
126 (molybdenite)-forming process. To the best of our knowledge, this is the first approach
127 evaluating the ore-forming fluid evolution path under an absolute timeframe.

128 A single sinusoidal quartz vein hosted by aplite (Fig. 2A, Fig. DR3A), which was formed
129 before the main mineralization stage (Li et al., 2017b), was analyzed to evaluate the fluid
130 nature prior to the main stage mineralization. Further, a total of 12 molybdenite bearing
131 quartz veins (Table DR1) with Re-Os dates (Li et al., 2017a) were analyzed by CL and SIMS
132 to yield successive generations of quartz and oxygen isotopic compositions, respectively. One
133 vein (1605-211) from (Li et al., 2017a) was not analyzed due to the inability to conform the
134 co-precipitated association between quartz grains and molybdenite samples.

To provide constraints on the oxygen isotopic composition of the original magmatic fluid during ore formation, magmatic zircon and quartz grains were separated from two fresh Rongmucuola monzogranite hand specimens, one from the west and the other from the east of the Rongmucuola pluton. The fresh samples from ore-bearing and barren parts of the pluton permitted the evaluation of potential variations of magmatic water oxygen isotopic composition during ore formation. The P porphyry was not used for this purpose as it has been intensive hydrothermally altered (Li et al., 2017a; Li et al., 2017b).

A3.2 Methods

Following the recovery during molybdenite separation, the quartz grains were cleaned and mounted with the NBS-28 and Qinghu quartz standards in epoxy resin, polished and then coated with gold (Li et al., 2017c). CL imaging was conducted with a Hitachi SU-70 SEM at Durham University (Li et al., 2017c). The imaging conditions were 15 kv, 100 nA and 20 mm for accelerating voltage, beam current and working distance, respectively, under a high vacuum mode. Secondary electron images were taken using the same conditions, but at a beam current of 1 nA.

Quartz SIMS oxygen isotope analysis was carried out at the Institute of Geology and Geophysics, Chinese Academy of Sciences with a CAMECA IMS-1280 SIMS (Li et al., 2010). The Cs^+ primary ion beam was accelerated at 10 kV, with an intensity of ca. 2 nA and rastered over a 20 μm area. The spot size as an ellipse was ~10 × 20 μm in diameter. Oxygen isotopes were measured using multi-collection mode on two off-axis Faraday cups, with the intensity of ^{16}O was typically 10^9 cps during this study. The instrumental mass fractionation factor (IMF) was corrected using NBS-28 with a $\delta^{18}O$ value (VSMOW) of 9.5 ‰ (Matsuhisa, 1974). Measured $^{18}O/^{16}O$ ratios were normalized to the VSMOW composition ($^{18}O/^{16}O$ = 0.0020052), and then corrected for the IMF. The uncertainty on individual analysis was

159 usually better than 0.3 - 0.4 ‰ (2SE). The studied samples were run during the same period
160 of a previous study (Li et al., 2017c), and the long-term drift during the course of study was
161 monitored by analyzing the Qinghu quartz standard between samples. The Qinghu standard
162 yields $\delta^{18}O$ values between 8.34 ± 0.23 and 8.92 ± 0.37 ‰ (Li et al., 2017c), with a mean of
163 8.64 ± 0.28 ‰ (2SD, n = 41). For each analysed quartz vein, CL images and the distribution
164 of $\delta^{18}O$ values are used to evaluate the potential presence of recognizable multiple growth
165 history. The analyzed positions are re-checked under a microscope, and analyses with the
166 presence of inclusions or offset from the target, e.g., away from the growth zonation, are
167 omitted. When single quartz growth history was demonstrated, e.g., no presence of
168 dissolution/resorption textures and homogeneous $\delta^{18}O$ values (e.g., Fig. 3, see below for
169 further details), it is interpreted that the weighted mean of the $\delta^{18}O$ values represents the best
170 estimate of the $\delta^{18}O$ value of that vein.

171 Experimentally determined quartz-water oxygen isotope fractionation equation
172 (equations 1 and 2) (Matsuhisa et al., 1979) was used to calculate the $\delta^{18}O$ values of ore-
173 forming fluid ($\delta^{18}O_{fluid}$). For fractionation calculation, hydrothermal and magmatic quartz
174 formation temperatures (T in unit of ^{o}C) were constrained by a previous quartz (molybdenite
175 bearing quartz veins) fluid inclusion study (Li et al., 2017b) and quartz-zircon equilibrium
176 oxygen isotope fractionation, respectively. Uncertainties of the $\delta^{18}O_{fluid}$ values were
177 calculated with propagation of uncertainties from $\delta^{18}O_{quartz}$ measurements and fluid inclusion
178 homogenization temperatures (± 20 ^{o}C) by Monte Carlo simulation.

179 $$\delta^{18}O_{quartz} - \delta^{18}O_{fluid} = 3.34 * (10^6 / (T + 273.15)^2) - 3.31 \quad 250\ ^{o}C < T < 500\ ^{o}C \qquad (1)$$

180 $$\delta^{18}O_{quartz} - \delta^{18}O_{fluid} = 2.05 * (10^6 / (T + 273.15)^2) - 1.14 \quad 500\ ^{o}C < T < 800\ ^{o}C \qquad (2)$$

To evaluate the percentage contribution (R) of magmatic water in the hydrothermal system, a binary mixing model with end members of meteoric water ($\delta^{18}O_{meteoric}$) and magmatic water ($\delta^{18}O_{magmatic}$), as presented in equation 3, was used.

$$\delta^{18}O_{fluid} = \delta^{18}O_{magmatic} * R + \delta^{18}O_{meteoric} * (1-R) \quad (3)$$

A4. Oxygen isotope equilibrium time between water and quartz

Here we further adjust the oxygen isotope equilibrium time between quartz and water. There is a lack of direct experimental studies to quantify the oxygen isotope exchange rate between quartz and water. Using the experimental study of a granite-fluid system (water/mineral ratio of 5, salinity of 5.8 wt. % NaCl equiv. and containing >22.6 wt. % quartz) as an alternative, with quartz of an average grain size of 0.4 cm (radius is 0.2 cm), oxygen isotope equilibrium can be achieved within 20 years (Fig. DR4B) at 300 ^{o}C (Cole et al., 1992). The experimental study further predicts a reduction in the equilibrium time with increased temperature, fluid salinity and water/mineral ratio.

A previous fluid inclusion study (Li et al., 2017b) suggests that the hydrothermal fluids at Qulong have formation temperatures of between 425 and 280 ^{o}C (average = 340 ^{o}C) with salinities of >5 wt. % NaCl equiv. (Table DR1). Considering the average Cu concentration in porphyry ore-forming fluid is ~0.1 wt.% (Landtwing et al., 2005; Kouzmanov and Pokrovski, 2012), the minimum volume of hydrothermal fluids to deposit the 11 Mt Cu at Qulong is >1.1×10^{10} m^3 assuming that the dissolved metals can be sufficiently and completely deposited. The Qulong deposit contains 2200 Mt of ore (Li et al., 2017b), which is equal to a volume of ~8×10^{8} m^3. The vein volume density in porphyry deposits is suggested to vary between 5 and 10 % in the ore shells (Weis et al., 2012), as such the maximum quartz volume at Qulong is estimated to be 8×10^{7} m^3. The minimum fluid volume and maximum quartz

volume estimated above suggest a minimum water/quartz ratio of 10 for Qulong. As discussed above, the growth temperature, fluid salinity and water/mineral ratio of hydrothermal quartz grains at Qulong (425 – 280 ^{o}C, >5 wt. %, 10) are favorable for the vein quartz to reach oxygen equilibrium with fluid if their growth time is longer than 20 years.

A5. References

Cole, D. R., Ohmoto, H., and Jacobs, G. K., 1992, Isotopic exchange in mineral-fluid systems: III. Rates and mechanisms of oxygen isotope exchange in the system granite-H2O ± NaCl ± KCl at hydrothermal conditions: Geochimica et Cosmochimica Acta, v. 56, no. 1, p. 445-466.

Hu, Y. B., Liu, J. Q., Ling, M. X., Ding, W., Liu, Y., Zartman, R. E., Ma, X. F., Liu, D. Y., Zhang, C. C., Sun, S. J., Zhang, L. P., Wu, K., and Sun, W. D., 2015, The formation of Qulong adakites and their relationship with porphyry copper deposit: Geochemical constraints: Lithos, v. 220, no. 0, p. 60-80.

Kouzmanov, K., and Pokrovski, G. S., 2012, Hydrothermal controls on metal distribution in porphyry Cu (-Mo-Au) systems: Special Publication of the Society of Economic Geologists, v. 16, no. 22, p. 573–618.

Landtwing, M. R., Pettke, T., Halter, W. E., Heinrich, C. A., Redmond, P. B., Einaudi, M. T., and Kunze, K., 2005, Copper deposition during quartz dissolution by cooling magmatic–hydrothermal fluids: The Bingham porphyry: Earth and Planetary Science Letters, v. 235, no. 1–2, p. 229-243.

Li, X. H., Li, W. X., Li, Q. L., Wang, X. C., Liu, Y., and Yang, Y. H., 2010, Petrogenesis and tectonic significance of the similar to 850 Ma Gangbian alkaline complex in South China: Evidence from in situ zircon U-Pb dating, Hf-O isotopes and whole-rock geochemistry: Lithos, v. 114, no. 1-2, p. 1-15.

Li, Y., Selby, D., Condon, D., and Tapster, S., 2017a, Cyclic magmatic-hydrothermal evolution in porphyry systems: High-precision U-Pb and Re-Os geochronology constraints from the Tibetan Qulong porphyry Cu-Mo deposit: Economic Geology, v. 112, no. 6.

Li, Y., Selby, D., Feely, M., Costanzo, A., and Li, X.-H., 2017b, Fluid inclusion characteristics and molybdenite Re-Os geochronology of the Qulong porphyry copper-molybdenum deposit, Tibet: Mineralium Deposita, v. 52, no. 2, p. 137–158.

Li, Y., Li, J. W., Li, X. H., Selby, D., Huang, G. H., Chen, L. J., and Zheng, K., 2017c, An Early Cretaceous carbonate replacement origin for the Xinqiao stratabound massive sulfide deposit, Middle-Lower Yangtze Metallogenic Belt, China: Ore Geology Reviews, v. 80, p. 985-1003.

Matsuhisa, Y., 1974, $^{18}O/^{16}O$ ratios for NBS-28 and some silicate reference samples: Geochem. J, v. 8, p. 103-107.

Matsuhisa, Y., Goldsmith, J. R., and Clayton, R. N., 1979, Oxygen Isotopic Fractionation in the System Quartz-Albite-Anorthite-Water: Geochimica Et Cosmochimica Acta, v. 43, no. 7, p. 1131-1140.

Pollington, A. D., Kozdon, R., Anovitz, L. M., Georg, R. B., Spicuzza, M. J., and Valley, J. W., 2016, Experimental calibration of silicon and oxygen isotope fractionations between quartz and water at 250°C by in situ microanalysis of experimental products

and application to zoned low δ30Si quartz overgrowths: Chemical Geology, v. 421, p. 127-142.
Richards, J. P., 2011, Magmatic to hydrothermal metal fluxes in convergent and collided margins: Ore Geology Reviews, v. 40, no. 1, p. 1-26.
Trail, D., Bindeman, I. N., Watson, E. B., and Schmitt, A. K., 2009, Experimental calibration of oxygen isotope fractionation between quartz and zircon: Geochimica Et Cosmochimica Acta, v. 73, no. 23, p. 7110-7126.
Valley, J. W., and Graham, C. M., 1996, Ion microprobe analysis of oxygen isotope ratios in quartz from Skye granite: Healed micro-cracks, fluid flow, and hydrothermal exchange: Contributions to Mineralogy and Petrology, v. 124, no. 3-4, p. 225-234.
Weis, P., Driesner, T., and Heinrich, C. A., 2012, Porphyry-copper ore shells form at stable pressure-temperature fronts within dynamic fluid plumes: Science, v. 338, no. 6114, p. 1613-1616.
Xiao, B., Qin, K. Z., Li, G. M., Li, J. X., Xia, D. X., Chen, L., and Zhao, J. X., 2012, Highly Oxidized Magma and Fluid Evolution of Miocene Qulong Giant Porphyry Cu-Mo Deposit, Southern Tibet, China: Resource Geology, v. 62, no. 1, p. 4-18.
Yang, Z. M., Hou, Z. Q., White, N. C., Chang, Z. S., Li, Z. Q., and Song, Y. C., 2009, Geology of the post-collisional porphyry copper-molybdenum deposit at Qulong, Tibet: Ore Geology Reviews, v. 36, no. 1-3, p. 133-159.
Zhao, J. X., Qin, K. Z., Xiao, B., McInnes, B., Li, G. M., Evans, N., Cao, M. J., and Li, J. X., 2016, Thermal history of the giant Qulong Cu-Mo deposit, Gangdese metallogenic belt, Tibet: Constraints on magmatic-hydrothermal evolution and exhumation: Gondwana Research, v. 36, p. 390-409.

Figure DR1

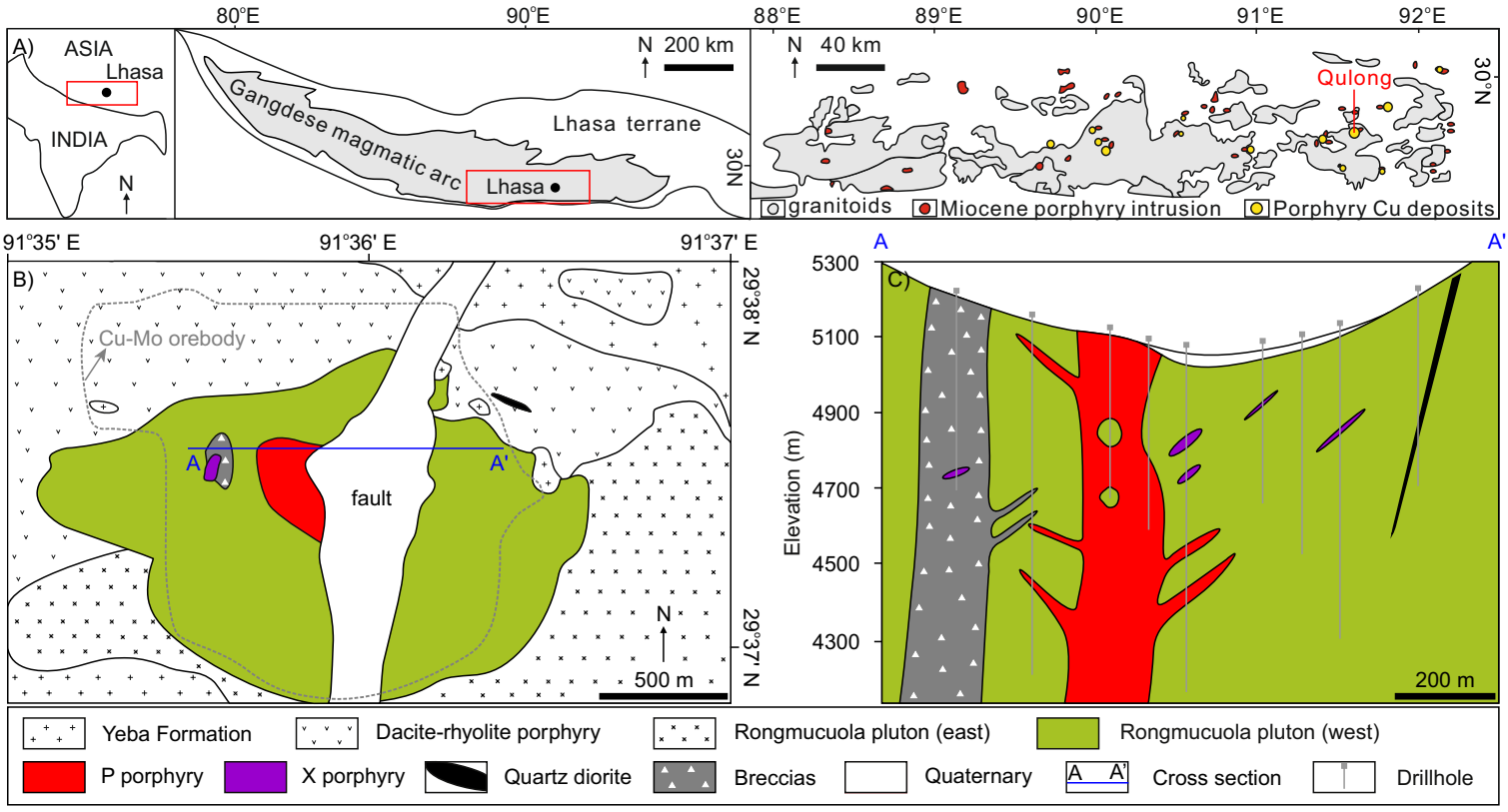
A)
ASIA
Lhasa
INDIA
N
80°E
90°E
N 200 km
Gangdese magmatic arc
Lhasa terrane
Lhasa
30°N
88°E
89°E
90°E
91°E
92°E
N 40 km
Qulong
30°N
granitoids
Miocene porphyry intrusion
Porphyry Cu deposits
B)
91°35' E
91°36' E
91°37' E
29°38' N
29°37' N
Cu-Mo orebody
A
A'
fault
N
500 m
C)
A
A'
5300
5100
4900
4700
4500
4300
Elevation (m)
200 m
Yeba Formation
Dacite-rhyolite porphyry
Rongmucuola pluton (east)
Rongmucuola pluton (west)
P porphyry
X porphyry
Quartz diorite
Breccias
Quaternary
A A'
Cross section
Drillhole

Figure DR2

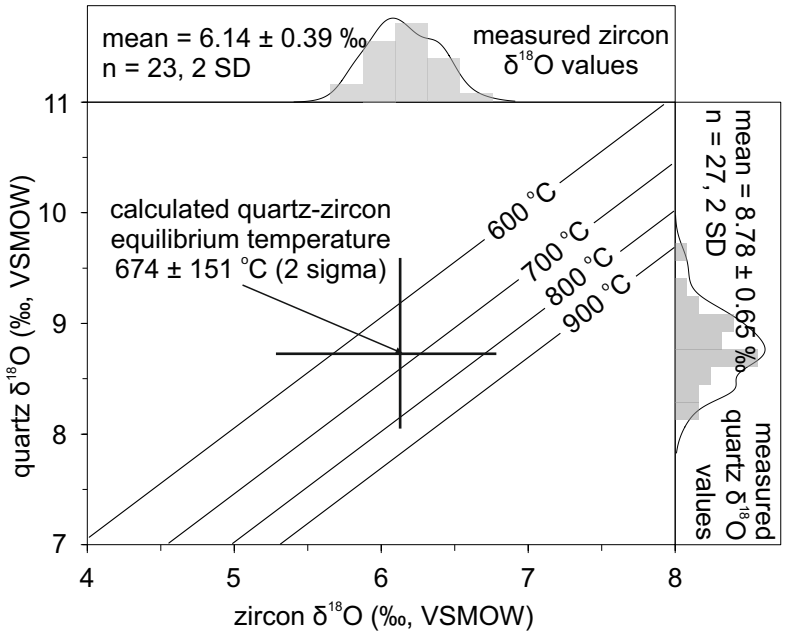
mean = 6.14 ± 0.39 ‰
n = 23, 2 SD
measured zircon
δ18O values
mean = 8.78 ± 0.65 ‰
n = 27, 2 SD
measured
quartz δ18O
values
calculated quartz-zircon
equilibrium temperature
674 ± 151 °C (2 sigma)
600 °C
700 °C
800 °C
900 °C
quartz δ18O (‰, VSMOW)
zircon δ18O (‰, VSMOW)
11
10
9
8
7
4
5
6
7
8

Figure DR3

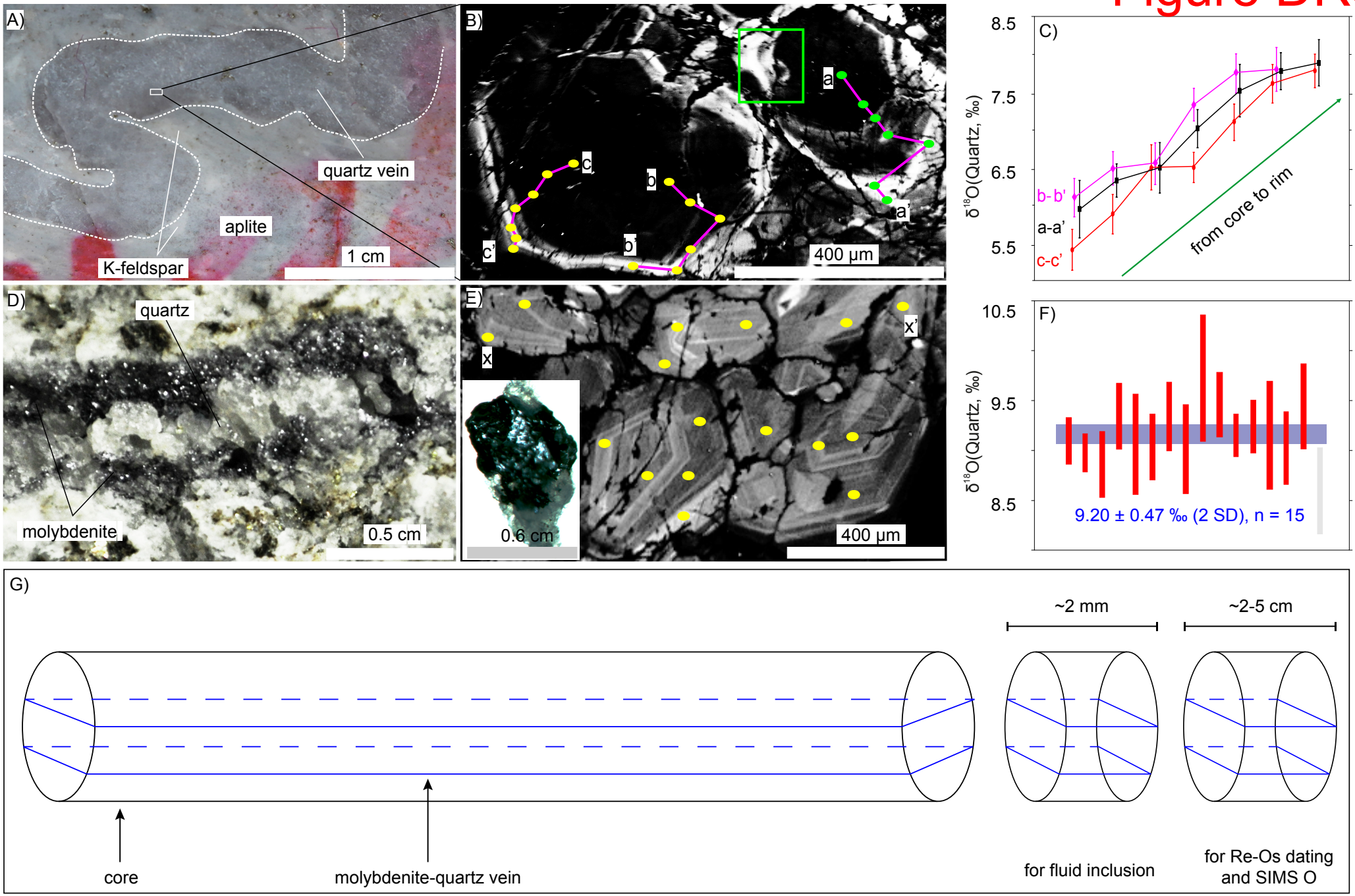
A)
quartz vein
aplite
K-feldspar
1 cm
B)
a
a'
b
b'
c
c'
400 μm
C)
8.5
7.5
6.5
5.5
δ18O(Quartz, ‰)
b-b'
a-a'
c-c'
from core to rim
D)
quartz
molybdenite
0.5 cm
E)
x
x'
0.6 cm
400 μm
F)
10.5
9.5
8.5
δ18O(Quartz, ‰)
9.20 ± 0.47 ‰ (2 SD), n = 15
G)
~2 mm
~2-5 cm
core
molybdenite-quartz vein
for fluid inclusion
for Re-Os dating
and SIMS O

Figure DR4

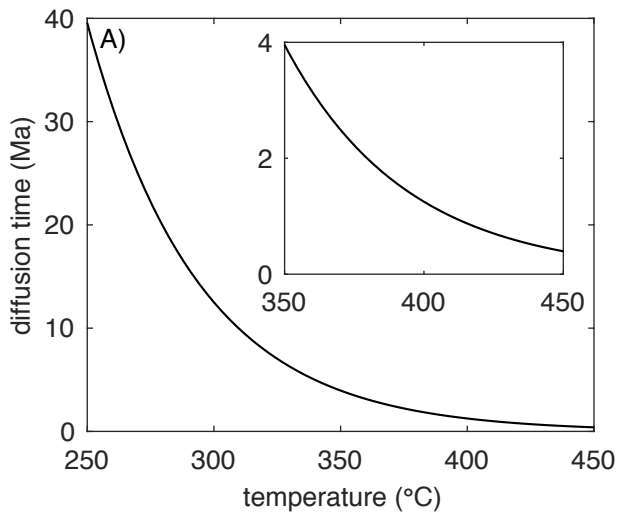
A)
diffusion time (Ma)
temperature (°C)
40
30
20
10
0
250
300
350
400
450
4
2
0
350
400
450

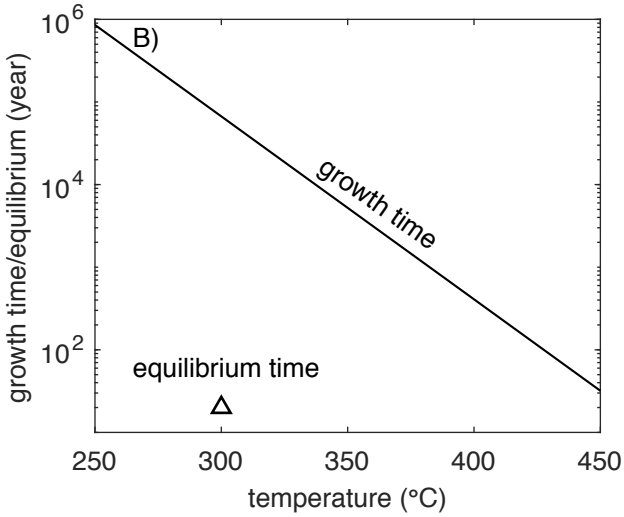
B)
growth time/equilibrium (year)
temperature (°C)
10^6
10^4
10^2
growth time
equilibrium time
250
300
350
400
450

Figure DR5

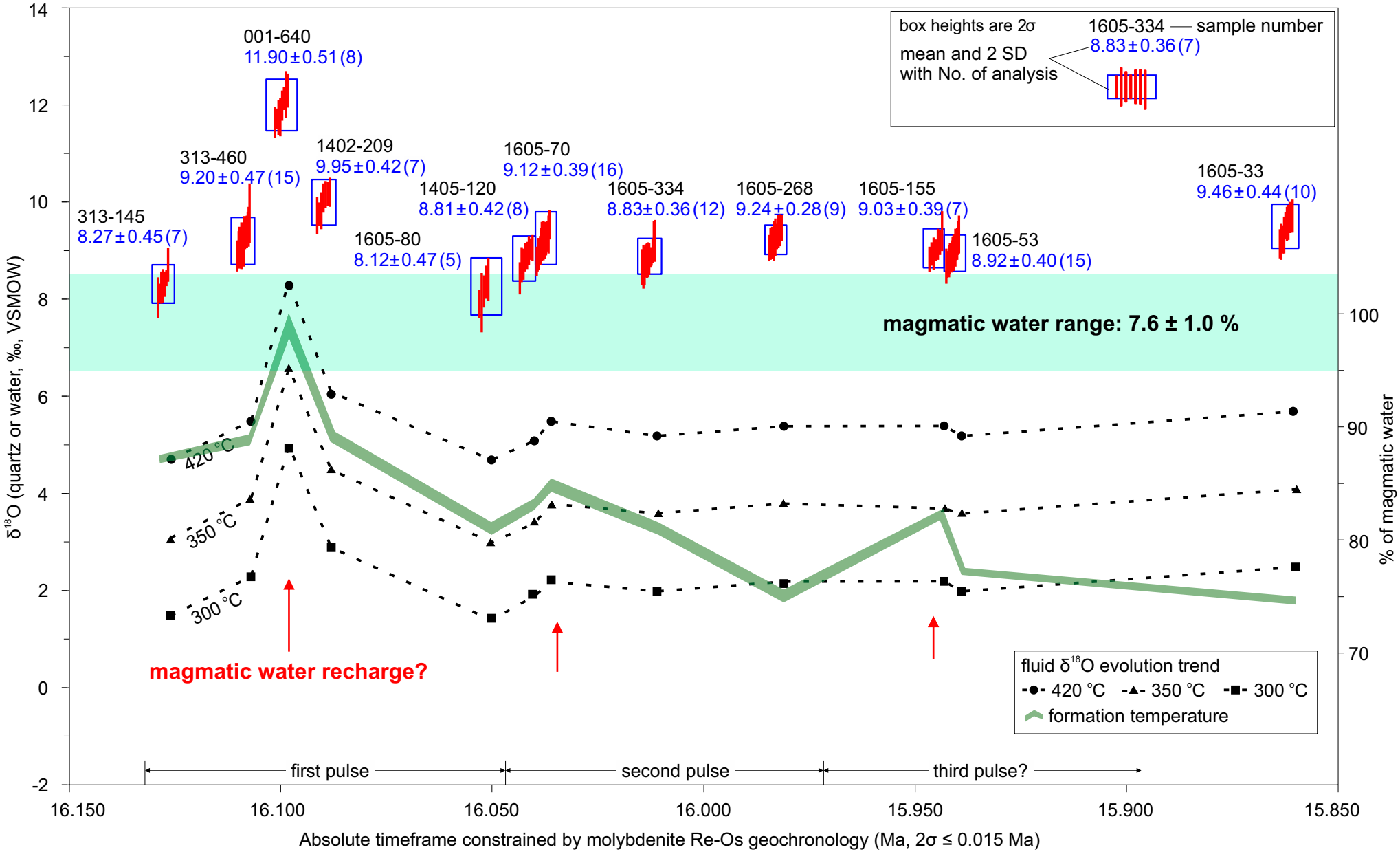
box heights are 2σ
mean and 2 SD
with No. of analysis
1605-334 — sample number
8.83±0.36(7)
001-640
11.90±0.51(8)
313-460
9.20±0.47(15)
1402-209
9.95±0.42(7)
313-145
8.27±0.45(7)
1605-80
8.12±0.47(5)
1405-120
8.81±0.42(8)
1605-70
9.12±0.39(16)
1605-334
8.83±0.36(12)
1605-268
9.24±0.28(9)
1605-155
9.03±0.39(7)
1605-53
8.92±0.40(15)
1605-33
9.46±0.44(10)
magmatic water range: 7.6 ± 1.0 %
420 °C
350 °C
300 °C
magmatic water recharge?
fluid δ18O evolution trend
420 °C
350 °C
300 °C
formation temperature
first pulse
second pulse
third pulse?
δ18O (quartz or water, ‰, VSMOW)
% of magmatic water
Absolute timeframe constrained by molybdenite Re-Os geochronology (Ma, 2σ ≤ 0.015 Ma)
14
12
10
8
6
4
2
0
-2
100
90
80
70
16.150
16.100
16.050
16.000
15.950
15.900
15.850

Table DR1. Oxygen isotopic composition of quartz grains enclosed by molybdenite, with estimations of fluid $\delta^{18}O$ and magmatic water contribution

Sample No.	Formation age[1]		Formation Temperature[2]		$\delta^{18}O_{quartz}$		$\delta^{18}O_{fluid}$ with formation T and magmatic water %[3]				$\delta^{18}O_{fluid}$ and magmatic % with upper, average and lower limit mineralization temperatures[4]								
							$\delta^{18}O_{fluid}$		magmatic water %		420 ± 20 °C			350 ± 20 °C			300 ± 20 °C		
											$\delta^{18}O_{fluid}$		magmatic	$\delta^{18}O_{fluid}$		magmatic	$\delta^{18}O_{fluid}$		magmatic
	Ma	2σ	°C	2σ	‰	2σ	‰	2σ	value	2σ	‰	2σ	water %	‰	2σ	water %	‰	2σ	water %
313-145	16.126	0.008	425	20	8.27	0.45	4.7	0.6	88%	5%	4.6	0.6	87%	3.0	0.7	80%	1.4	0.8	73%
313-460	16.107	0.015	398	20	9.20	0.47	5.1	0.6	89%	5%	5.6	0.6	91%	3.9	0.7	84%	2.3	0.9	77%
001-640	16.098	0.013	390	20	11.90	0.51	7.6	0.7	100%	5%	8.3	0.6	103%	6.6	0.8	96%	5.0	0.9	89%
1402-209	16.088	0.007	380	20	9.95	0.42	5.4	0.6	91%	5%	6.3	0.6	94%	4.7	0.7	87%	3.1	0.8	80%
1605-80	16.050	0.005	360	20	8.12	0.47	3.1	0.7	81%	6%	4.5	0.6	87%	2.8	0.7	79%	1.3	0.9	73%
1405-120	16.040	0.007	365	20	8.81	0.42	3.9	0.7	84%	5%	5.2	0.6	90%	3.5	0.7	82%	1.9	0.8	76%
1605-70	16.036	0.012	365	20	9.12	0.39	4.2	0.6	85%	5%	5.5	0.6	91%	3.8	0.7	84%	2.3	0.8	77%
1605-334	16.011	0.015	340	20	8.83	0.36	3.2	0.7	81%	6%	5.2	0.5	90%	3.5	0.7	82%	2.0	0.8	76%
1605-268	15.981	0.007	290	20	9.24	0.28	2.0	0.8	76%	6%	5.6	0.5	91%	3.9	0.6	84%	2.4	0.8	77%
1605-155	15.943	0.007	345	20	9.03	0.39	3.6	0.7	83%	5%	5.4	0.6	90%	3.7	0.7	83%	2.2	0.8	76%
1605-53	15.939	0.006	310	20	8.92	0.40	2.4	0.8	78%	6%	5.3	0.6	90%	3.6	0.7	83%	2.1	0.8	76%
1605-33	15.860	0.010	280	20	9.46	0.44	1.8	0.9	75%	6%	5.8	0.6	92%	4.2	0.7	85%	2.6	0.8	78%

1. Formation ages are constrained by molybdenite Re-Os geochronology from Li et al., 2017a.
2. Formation temperatures are constrained by trapping T of fluid inclusion group from the parellel wafers of the veins Li et al., 2017b.
3. Magmaic water and meteoric water $\delta^{18}O$ values are 7.6 ± 1.0 ‰ (this study) and -15.6 ± 3.6 ‰ (Currie et al., 2005), respectively.
4. To test the robustness of the temperatures used for oxygen isotope calculation, the uper, average and lower limit of mineralization temperatures represent mineralization temperature variations at Qulong and typical PCDs are used for testing.

Table DR2. SIMS $\delta^{18}O$ values of zircon and groundmass quartz of the Rongmucuola pluton

Sample NO.	$\delta^{18}O$	2σ	Mean and 2 SD (‰, VSMOW)	
Zircon sample				
QL14_23W@1	6.43	0.19		
QL14_23W@2	6.00	0.18		
QL14_23W@3	5.82	0.16		
QL14_23W@5	5.92	0.28	QL14_23W	
QL14_23W@6	6.44	0.21	Mean = 6.14 ± 0.46, n = 11.	
QL14_23W@7	6.37	0.17		
QL14_23W@8	5.80	0.26		
QL14_23W@9	6.10	0.26		
QL14_23W@10	6.28	0.25		
QL14_23W@11	6.16	0.32		QL14_23W + QL14_52E
QL14_23W@12	6.19	0.29		
QL14_52E@1	6.17	0.26		Mean = 6.14 ± 0.39, n = 23.
QL14_52E@2	5.99	0.21		
QL14_52E@3	6.12	0.22		
QL14_52E@4	6.01	0.32		
QL14_52E@5	5.99	0.27		
QL14_52E@6	~~6.55~~	~~0.29~~	QL14_52E	
QL14_52E@7	6.01	0.29	Mean = 6.14 ± 0.34, n = 12.	
QL14_52E@10	6.18	0.25		
QL14_52E@11	6.21	0.32		
QL14_52E@12	5.94	0.42		
QL14_52E@13	6.50	0.45		
QL14_52E@14	6.13	0.23		
QL14_52E@15	6.38	0.22		
quartz sample				
QL14_23W@1	8.49	0.36		
QL14_23W@3	9.12	0.22		
QL14_23W@4	8.95	0.29		
QL14_23W@5	8.45	0.29		
QL14_23W@8	9.05	0.33	QL14_23W	
~~QL14_23W@9~~	~~9.99~~	~~0.22~~	Mean = 8.83 ± 0.83, n = 12.	
QL14_23W@10	8.74	0.25		
QL14_23W@11	8.87	0.30		
QL14_23W@12	9.38	0.46		
QL14_23W@13	8.79	0.30		
QL14_23W@14	9.56	0.31		
QL14_23W@15	8.40	0.16		QL14_23W + QL14_52E
QL14_23W@16	8.16	0.36		
QL14_52E@2	8.69	0.21		Mean = 8.78 ± 0.65, n = 27.
QL14_52E@3	8.60	0.35		
QL14_52E@4	8.96	0.31		
QL14_52E@5	8.97	0.35		
~~QL14_52E@7~~	~~7.03~~	~~0.27~~		
QL14_52E@10	8.91	0.32		
QL14_52E@11	8.59	0.35		
QL14_52E@12	8.70	0.50	QL14_52E	
QL14_52E@13	9.21	0.39	Mean = 8.74 ± 0.48, n = 15.	
~~QL14_52E@15~~	~~9.68~~	~~0.22~~		
QL14_52E@16	8.93	0.28		
QL14_52E@17	8.71	0.32		
QL14_52E@18	8.60	0.29		
QL14_52E@19	8.73	0.29		
QL14_52E@20	8.38	0.22		
QL14_52E@21	8.26	0.31		
QL14_52E@22	8.81	0.35		

QL14_23W and QL14_52E are relative fresh samples from the west and east of the Rongmucuola pluton, respectively.

Data do not belong to the main population are rejected (with strikethough) and are not used for mean value caculations

Table DR3. SIMS $\delta^{18}O$ values of hydrothermal quartz from Qulong

Sample No.	$\delta^{18}O$	2σ		
Sinusoidal like quartz vein				
Section A				
817-290@A1	5.95	0.38		
817-290@A2	6.33	0.22		
817-290@A3	6.50	0.33		
817-290@A4	7.01	0.25		
817-290@A5	7.52	0.35		
817-290@A6	7.78	0.24		
817-290@A7	7.89	0.31		
Section B				
817-290@B1	6.11	0.26		
817-290@B2	6.49	0.22		
817-290@B3	6.55	0.28		
817-290@B4	7.33	0.22		
817-290@B5	7.75	0.27		
817-290@B6	7.80	0.29		
Section C				
817-290@C1	5.40	0.27		
817-290@C2	5.88	0.26		
817-290@C3	6.49	0.30		
817-290@C4	6.50	0.20		
817-290@C5	7.10	0.24		
817-290@C6	7.61	0.26		
817-290@C7	7.78	0.22		
Molybdenite bearing veins				
Sample No.	$\delta^{18}O$	2σ	average	2 SD
313-145@1	8.09	0.20	8.27	0.45
313-145@2	8.41	0.17	n=7	
313-145@4	8.00	0.42		
313-145@5	8.28	0.26		
313-145@6	8.21	0.33		
313-145@9	8.24	0.35		
313-145@10	8.68	0.35		
313-460@1	9.10	0.22	9.20	0.47
313-460@2	8.99	0.19	n=15	

313-460@3	8.85	0.31		
313-460@4	9.36	0.32		
313-460@5	9.07	0.48		
313-460@6	9.05	0.32		
313-460@7	9.36	0.33		
313-460@8	9.03	0.43		
313-460@9	9.74	0.61		
313-460@10	9.46	0.31		
313-460@11	9.16	0.20		
313-460@12	9.25	0.25		
313-460@13	9.16	0.52		
313-460@14	9.03	0.34		
313-460@15	9.46	0.41		
001-640@1	12.10	0.24	11.90	0.51
001-640@2	12.26	0.35	n=8	
001-640@4	11.68	0.21		
001-640@5	11.71	0.39		
001-640@7	12.18	0.48		
001-640@8	11.61	0.32		
001-640@9	11.95	0.31		
001-640@10	11.70	0.36		
1402-209@1	10.17	0.30	9.95	0.42
1402-209@3	9.79	0.38	n=7	
1402-209@4	9.69	0.38		
1402-209@5	9.72	0.24		
1402-209@8	10.14	0.25		
1402-209@9	10.12	0.28		
1402-209@11	10.05	0.30		
1605-80@2	7.87	0.29	8.12	0.47
1605-80@3	8.32	0.34	n=5	
1605-80@5	7.90	0.61		
1605-80@6	8.13	0.33		
1605-80@8	8.38	0.44		
1405-120@1	8.69	0.32	8.81	0.42
1405-120@2	8.40	0.33	n=8	
1405-120@3	8.97	0.30		
1405-120@4	8.87	0.28		
1405-120@5	9.02	0.27		
1405-120@6	8.68	0.36		
1405-120@7	8.83	0.29		

1405-120@8	9.00	0.22		
1605-70@1	9.26	0.31	9.12	0.39
1605-70@2	9.28	0.25	n=16	
1605-70@3	8.97	0.24		
1605-70@4	9.50	0.30		
1605-70@5	9.01	0.26		
1605-70@6	8.75	0.30		
1605-70@7	8.90	0.33		
1605-70@8	9.21	0.34		
1605-70@9	9.16	0.40		
1605-70@10	9.05	0.38		
1605-70@11	9.18	0.34		
1605-70@12	9.18	0.38		
1605-70@13	9.17	0.24		
1605-70@16	8.78	0.24		
1605-70@17	9.17	0.40		
1605-70@18	9.30	0.39		
1605-334@1	8.76	0.34	8.83	0.36
1605-334@2	9.17	0.43	n=12	
1605-334@3	8.84	0.18		
1605-334@4	8.64	0.45		
1605-334@6	9.16	0.41		
1605-334@7	8.63	0.37		
1605-334@11	8.66	0.39		
1605-334@12	8.97	0.25		
1605-334@13	8.78	0.36		
1605-334@15	8.80	0.33		
1605-334@16	8.77	0.36		
1605-334@17	8.83	0.21		
1605-268@2	9.26	0.26	9.24	0.28
1605-268@3	9.17	0.41	n=9	
1605-268@4	9.13	0.33		
1605-268@7	9.37	0.34		
1605-268@8	9.43	0.27		
1605-268@9	9.39	0.33		
1605-268@10	9.11	0.33		
1605-268@11	9.02	0.27		
1605-268@13	9.24	0.39		
1605-155@1	9.37	0.41	9.03	0.39
1605-155@2	8.91	0.33	n=7	

1605-155@3	8.98	0.22		
1605-155@4	9.14	0.26		
1605-155@6	9.10	0.32		
1605-155@7	8.79	0.26		
1605-155@9	8.90	0.24		
1605-53@3	8.68	0.28	8.92	0.40
1605-53@4	8.92	0.34	n=15	
1605-53@5	8.82	0.23		
1605-53@6	8.92	0.37		
1605-53@7	9.23	0.35		
1605-53@8	9.05	0.28		
1605-53@9	9.30	0.39		
1605-53@10	8.70	0.25		
1605-53@12	9.11	0.33		
1605-53@13	9.03	0.39		
1605-53@14	8.80	0.32		
1605-53@15	8.75	0.33		
1605-53@16	8.65	0.36		
1605-53@17	8.85	0.33		
1605-53@19	9.00	0.30		
1605-33@1	9.15	0.37	9.46	0.44
1605-33@2	9.20	0.29	n=10	
1605-33@3	9.29	0.38		
1605-33@4	9.52	0.35		
1605-33@5	9.11	0.30		
1605-33@8	9.68	0.34		
1605-33@10	9.55	0.36		
1605-33@12	9.65	0.32		
1605-33@14	9.48	0.28		
1605-33@16	9.65	0.31		

Data do not belong to the main population or show evidence of mineral inclusions, or located at wrong targets after reexamination are rejected (with strikethough), and thus are not used for mean values calculation.